Theor Chem Acc (2011) 130:197–207
DOI 10.1007/s00214-011-0959-z

REGULAR ARTICLE

The role of the heteroatom (X = Si^{IV}, P^{V}, and S^{VI}) on the reactivity of $\{\gamma$-$[(H_2O)Ru^{III}(\mu$-$OH)_2Ru^{III}(H_2O)][X^{n+}W_{10}O_{36}]\}^{(8-n)-}$ with the O_2 molecule

Aleksey E. Kuznetsov · Yurii V. Geletii · Craig L. Hill · Keiji Morokuma · Djamaladdin G. Musaev

Received: 24 February 2011 / Accepted: 10 May 2011 / Published online: 25 May 2011

Abstract The mechanism of reaction of the di-Ru-substituted polyoxometalate, $\{\gamma$-$[(H_2O)Ru^{III}(\mu$-$OH)_2Ru^{III}(H_2O)][X^{n+}W_{10}O_{36}]\}^{(8-n)-}$, **I_X**, with O_2, i.e. **I_X** + O_2 → $\{\gamma$-$[(O)Ru^{IV}(\mu$-$OH)_2Ru^{IV}(O)][X^{n+}W_{10}O_{36}]\}^{(8-n)-}$ + $2H_2O$, (1), was studied at the B3LYP density functional and self-consistent reaction field IEF-PCM (in aqueous solution) levels of theory. The effect of the nature of heteroatom X (where X = Si, P and, S) on the calculated energies and mechanism of the reaction (1) was elucidated. It was shown that the nature of X only slightly affects the reactivity of **I_X** with O_2, which is a 4-electron oxidation process. The overall reaction (1): (a) proceeds with moderate energy barriers for all studied X's [the calculated rate-determining barriers are X = Si (18.7 kcal/mol) < S (20.6 kcal/mol) < P (27.2 kcal/mol) in water, and X = S (18.7 kcal/mol) < P (21.4 kcal/mol) < Si (23.1 kcal/mol) in the gas phase] and (b) is exothermic [by X = Si [28.7 (22.1) kcal/mol] > P [21.4 (9.8) kcal/mol] > S [12.3 (5.0) kcal/mol]. The resulting $1\{\gamma-[(O)Ru^{IV}(\mu-OH)_2Ru^{IV}(O)][X^{n+}W_{10}O_{36}]\}^{(8-n)-}$, **VI_X**, complex was found to have two $Ru^{IV}=O$ units, rather than $Ru^{V}=O$ units. The "reverse" reaction, i.e., water oxidation by **VI_X** is an endothermic process and unlikely to occur for X = Si and P, while it could occur for X = S under specific conditions. The lack of reactivity of **VI_X** biradical toward the water molecule leads to the formation of the stable $[\{Ru_4^{IV}O_4(OH)_2(H_2O)_4\}[(\gamma$-$XW_{10}O_{36}]_2\}^{m-}$ dimer. This conclusion is consistent with our experimental findings; previously we prepared the $[\{Ru_4^{IV}O_4(OH)_2(H_2O)_4\}[(\gamma-XW_{10}O_{36}]_2\}^{m-}$ dimers for X = Si (m = 10) [Geletii et al. in Angew Chem Int Ed 47:3896–3899, 2008 and J Am Chem Soc 131:17360–17370, 2009] and P (m = 8) [Besson et al. in Chem Comm 46:2784–2786, 2010] and showed them to be very stable and efficient catalysts for the oxidation of water to O_2.

Keywords Density functional · Catalysis · Polyoxometalate · Water oxidation

1 Introduction

The stability and versatility of polyoxometalates (POM), as well as the tunability of their size, charge, composition, and redox properties, make them attractive for applications in catalysis and many other areas [1–7]. Polyoxometalates with multinuclear d-electron-containing centers capable of accepting several electrons in conjunction with oxidation processes have attracted considerable attention [8–17]. Very recently, we performed detailed computational studies on the mechanism and governing factors of O_2 activation by the di-Ru-substituted γ-Keggin polyoxotungstate $\{\gamma-[(H_2O)Ru^{III}(\mu-OH)_2Ru^{III}(H_2O)][SiW_{10}O_{36}]\}^{4-}$, **I_Si** [18] (throughout this paper, we use the following notations:

Dedicated to Professor Shigeru Nagase on the occasion of his 65th birthday and published as part of the Nagase Festschrift Issue.

Electronic supplementary material The online version of this article (doi:10.1007/s00214-011-0959-z) contains supplementary material, which is available to authorized users.

A. E. Kuznetsov · Y. V. Geletii · C. L. Hill · K. Morokuma · D. G. Musaev (✉)
Cherry L. Emerson Center for Scientific Computation and Department of Chemistry, Emory University, 1515 Dickey Drive, Atlanta, GA 30322, USA
e-mail: dmusaev@emory.edu

Present Address:
A. E. Kuznetsov
Chemistry Department, Duke University, 124 Science Drive, Box 90354, Durham, NC 27708, USA

N_X or **TSn_X**, where **N** corresponds to an intermediate, **TSn** stands for a transition state, and **X** = Si, P, or S stands for the heteroatom). These studies showed that the 4-electron oxidation of **I_Si** by O_2 is a highly exothermic $[\Delta E_{gas} = -28.7 (\Delta E_{gas} + \Delta G_{solv(water)} = -22.1)$kcal/mol] reaction and leads to the formation of $\{\gamma-[(^{\cdot}O)Ru^{IV}(\mu-OH)_2Ru^{IV}(O^{\cdot})][SiW_{10}O_{36}]\}^{4-}$, **VI_Si**, and two water molecules. It proceeds via: (1) an H_2O-to-O_2 substitution that occurs with a maximum barrier of 23.1 (10.5) kcal/mol and leads to the formation of a water molecule and $\{\gamma-[(OO)Ru^{IV}(\mu-OH)_2Ru^{III}(H_2O)][SiW_{10}O_{36}]\}^{4-}$, **III_Si**, complex with a superoxide ($OO^{-\cdot}$) ligand (the first 1 e-oxidation); (2) a proton transfer from the coordinated H_2O molecule to the superoxide ($OO^{-\cdot}$) unit in **III_Si** to form a hydroperoxo-hydroxo intermediate $\{\gamma$-$[(OOH)Ru^{IV}(\mu$-$OH)_2Ru^{IV}(OH)][SiW_{10}O_{36}]\}^{4-}$, **IV-1_Si** (the second 1 e-oxidation); (3) the O-OH bond cleavage followed by the spontaneous formation of a water molecule and (H_2O) $\{\gamma-[(^{\cdot}O)Ru^{IV}(\mu-OH)_2Ru^{IV}(O^{\cdot})][SiW_{10}O_{36}]\}^{4-}$, **V_Si**, containing two $Ru^{IV} = O^{\cdot}$ bonds; and (4) dissociation of the H-bound water molecule from **V_Si** to form the $\{\gamma$-$[(^{\cdot}O)Ru^{IV}(\mu$-$OH)_2Ru^{I-V}(O^{\cdot})][SiW_{10}O_{36}]\}^{4-}$, **VI_Si**, product. Each of these elementary steps (except (4)) is exothermic and occurs with a moderate energy barrier.

The reverse reaction, water oxidation by **VI_Si**, was found to be a highly endothermic and therefore an unfeasible process; this finding is different from that reported for the "blue-dimer" intermediate, $\{(bpy)_2[(^{\cdot}O)Ru^{IV}(\mu$-$O)Ru^{I-V}(O^{\cdot})](bpy)_2\}^{4+}$, which readily oxidizes an incoming water molecule to produce O_2 [19–32]. The main reason for this difference between **VI_Si** and its "blue-dimer" analog in reactivity toward the water molecule was shown [18] to be the high stability of **VI_Si** compared with the analogous "blue-dimer" intermediate relative to the O_2 formation, which in turn was found to derive from the electron-rich nature of $[SiW_{10}O_{36}]^{4-}$ compared to *bpy* ligands.

Recently, the role of the heteroatom *X* in stability and reactivity of the di-transition-metal substituted γ-Keggin polyoxometalates $\{\gamma$-$[M(\mu$-$OH)_2M][X^{n+}(M_{FW})_{10}O_{36}]\}^{(8-n)-}$ was computationally investigated for $X = Al^{III}$, Si^{IV}, P^{V}, and S^{VI}, M = Fe, Mn, and Ru, and M_{FW} = Mo and W [33, 34]. It was shown that the change in *X* via Al^{III}–Si^{IV}–P^{V}–S^{VI} slightly stabilizes the broken-symmetry (BS) state over the high-spin (HS) state, increases the antiferromagnetic coupling constant, *J*, and lowers the energies of the HOMOs and LUMOs of these species. As a result, the oxidizing power of $\{\gamma$-$[M(\mu$-$OH)_2M][X^{n+}(M_{FW})_{10}O_{36}]\}^{(8-n)-}$ is expected to increase via $X = Al < Si < P < S$.

The present paper is a continuation of our previous studies [18, 33–35] and addresses the effect of the heteroatom *X* on the mechanism and energetics of the reaction:

$$\{\gamma - [(H_2O)Ru^{III}(\mu - OH)_2Ru^{III}(H_2O)][X^{n+}W_{10}O_{36}]\}^{(8-n)-} + O_2 \rightarrow \{\gamma - [(^{\cdot}O)Ru^{IV}(\mu - OH)_2Ru^{IV}(O^{\cdot})][X^{n+}W_{10}O_{36}]\}^{(8-n)-} + 2H_2O \quad (1)$$

for X = Si, [18] P and S (and n = 4, 3 and 2, respectively).

2 Computational details

All calculations were made using the Gaussian 03 program [36]. The geometries of all species under investigation were optimized without any symmetry constraint at the B3LYP/Lanl2dz level of theory with additional d polarization functions for the *X* atom ($\alpha = 0.55$) and the corresponding Hay–Wadt effective core potentials (ECPs) for W and Ru [37–42]. This method is subsequently referred to as "B3LYP/[Lanl2dz + d(*X*)]." The energetics of the optimized structures were further refined by performing single-point energy calculations using the Stuttgart pseudopotentials [43] and associated SDD basis sets for W and Ru and the standard 6 − 31 + G* split-valence-polarization basis set for all other atoms. This method will be subsequently referred to as "B3LYP/SDD." Antiferromagnetic exchange coupling constants (*J*) of the selected structures were calculated by utilizing Yamaguchi-Noodleman approach [44–47].

Previously, we have demonstrated that the B3LYP/[Lanl2dz + d(*X*)] approach reasonably describes the electronic and geometrical property of di-transition metal substituted Keggin-POM's [33, 34, 48]. Single-point B3LYP/SDD calculations of energies at the B3LYP/[Lanl2dz + d(*X*)] optimized geometries provide a better agreement with the available experiments [49].

Hessians were calculated only for transition states and confirmed to have one imaginary frequency corresponding to the reaction coordinate. The solvent effects were estimated at the B3LYP/SDD level of theory using the self-consistent reaction field IEF-PCM method [50] (UAKS model) by choosing water as a solvent (dielectric constant $\varepsilon = 78.39$). Below, we discuss gas-phase energetics ΔE (without zero-point correction) calculated at the B3LYP/SDD level of theory, as well as the energies including solvent effects $\Delta E + \Delta G_{solv}$ in parentheses. The Cartesian coordinates of all optimized structures at the B3LYP/[Lanl2dz + d(*X*)] level along with the results of their full Mulliken analysis are presented in Supporting Information (Tables S1, S4 and S5).

One should note that about 81–84% (*X* = P) or 68–74% (*X* = S) of the solvation energy is due to electrostatic interactions between the solute and solvent. Non-electro-

static components (including cavitation, dispersion, and repulsion energies) of this energy are within 16–19% ($X = P$) or 32–26% ($X = S$) for all the calculated structures (see Tables S2 and S3 of Supporting Information).

3 Results

3.1 Geometry and electronic structure of the reactant complexes

The reactant of the reaction (1) is a bis-aqua species $\{\gamma\text{-}[(H_2O)Ru^{III}(\mu\text{-}OH)_2Ru^{III}(H_2O)][X^{n+}W_{10}O_{36}]\}^{(8-n)-}$, **I_X**. Previously, we showed for **I_Si** that this complex may have several different isomers, which differ by the position of the water molecules [18]. The structure of the energetically most stable isomer of **I_Si**, along with its most important geometry parameters, is presented in Fig. 1.

For **I_P** and **I_S**, we investigate only the same (as **I_Si**) isomers. Similar to **I_Si**, the **I_P** and **I_S** species are calculated to have a singlet ground electronic state. As seen in Fig. 1, all three **I_X** species, in their ground singlet electronic state, have water molecules that (a) form hydrogen bonds with μ-OH and framework O (located between Ru and W atoms) centers of the POM and (b) coordinate to the Ru centers by their oxygen atoms. The orbitals involved in the $Ru–O_{H_2O}$ interaction are the bonding/antibonding combinations of d_{xz}- and d_{z2}-AOs of the Ru centers and p_z-AO of water molecule (see Figure S1 of Supporting Materials). The calculated $Ru^1–O^1$, $O^5–H^1$, $O^6–H^2$, $Ru^2–O^2$, $O^7–H^3$, and $O^8–H^4$ bond distances are 2.19, 2.01, 2.02, 2.28, 2.08 and 2.06, respectively, for $X = Si$, 2.13, 2.08, 2.09, 2.19, 2.23 and 2.23 Å, respectively, for $X = P$, and 2.09, 2.15, 2.17, 2.12, 2.49 and 2.49 Å, respectively, for $X = S$. The average $Ru–O_{H_2O}$ bond distance is 2.23, 2.16, and 2.11 Å, for complexes **I_Si, I_P**, and **I_S,** respectively. These values lie well within the range of $M–O_{H_2O}$ bond distances found for other POM compounds [51–57] and reduce as $X = Si > P > S$. Shortening of $Ru–O_{H_2O}$ for $X = P$ and especially S is consistent with the stabilization of the $Ru–O_{H_2O}$ bonding orbitals as $X = Si–P–S$: E(HOMO) = 0.09802 (Si), −0.00576 (P), and −0.11029 hartree (S) (see Figure S1 of Supporting Materials). In addition, these trends are consistent with the decrease in total negative charge of the **I_X** species [via $X = Si$ (−4) > P (−3) > S (−2)] via the same order.

It is worthwhile to notice the existence of low-lying triplet states of **I_P** and **I_S** species with geometries quite close to those of the singlet structures (excluding the $Ru^1–Ru^2$ and $O^5–O^6$ bond distances, see Figure S2 of Supporting Materials). For $X = P$ and S, these triplet species are located 3.6 (8.0) and 2.3 (5.3) kcal/mol higher than the singlet state, respectively. The septet states of **I_X** are 14.4 (38.4), 19.6 (39.0), and 14.3 (29.5) kcal/mol higher in energy than the singlet ground states, for $X =$ Si, P, and S, respectively.

3.2 Intermediates, transition states, and products of the reaction (1)

As shown previously [18], the first step of the reaction (1) is the substitution of one water molecule in **I_X** by O_2 to form the intermediate with a $\{(O_2)Ru^{IV}(\mu\text{-}OH)_2Ru^{III}(H_2O)\}$ core. As seen in Fig. 1, ligand environments of Ru^1 and Ru^2 atoms in **I_X** are different. Therefore, it is expected that O_2 will substitute the H_2O ligand on Ru^2. In general, this substitution reaction may proceed via stepwise and concerted pathways (also called the dissociative and associative pathways). The stepwise pathway occurs in two steps: (1) dissociation of water molecule from **I_X** to form $\{\gamma\text{-}Ru^{III}(\mu\text{-}OH)_2Ru^{III}(H_2O)][X^{n+}W_{10}O_{36}]\}^{(8-n)-}$, **II_X**, and (2) addition of O_2 to Ru^2 to form complex $\{\gamma\text{-}[(O_2)Ru^{IV}(\mu\text{-}OH)_2Ru^{III}(H_2O)][X^{n+}W_{10}O_{36}]\}^{(8-n)-}$, **III_X**. In the concerted pathway, substitution of water by O_2 occurs in a single step via a H_2O-to-O_2 substitution transition state. Previously [18], we have shown that the major conclusions obtained from the studies of both stepwise and concerted pathways are the same. Therefore, here we report the calculated intermediates and transition states of only computationally less-demanding stepwise/dissociative pathway of reaction (1).

3.2.1 *Intermediate **II_X**: the water dissociation from **I_X***

The first step of this pathway is the dissociation of one of the water molecules from **I_X** to give complex **II_X**. The ground electronic states of the resulting **II_P** and **II_S** species are found to be quintet states, not the singlet state as found for **II_Si** previously [18]. The calculated $\langle S^2 \rangle$ values are 6.02 for both **II_P** and **II_S** structures. The singlet, triplet, and septet states of these species lie by 3.4 (−1.2, i.e. inclusion of solvent effects makes the singlet state a slightly more favorable than the quintet state), 6.7 (12.0) and 6.2 (15.1) kcal/mol higher for **II_P**, and 11.1 (8.6), 13.0 (14.4) and 3.5 (10.3) kcal/mol higher for **II_S**, respectively. If we consider the ground state-to-ground state process, then the water dissociation from **I_X** would require 21.4 (13.4) and 18.7 (16.8) kcal/mol of energy (see Figs. 1, 2) for $X = P$ and S, respectively, which compare with 23.1 (10.5) kcal/mol found for $X = Si$ [18]. Thus, the endothermicity of this step decreases via $X = Si > P > S$ in the gas phase, but increases via the same order in the water solution.

As seen in Fig. 1, the geometry of the resulting *quintet* **II_P** and **II_S** species is significantly distorted. Indeed, in **II_P/II_S**, the $Ru^1–Ru^2$, $Ru^1–O^1$, $Ru^1–O_X$ and $Ru^2–O_X$

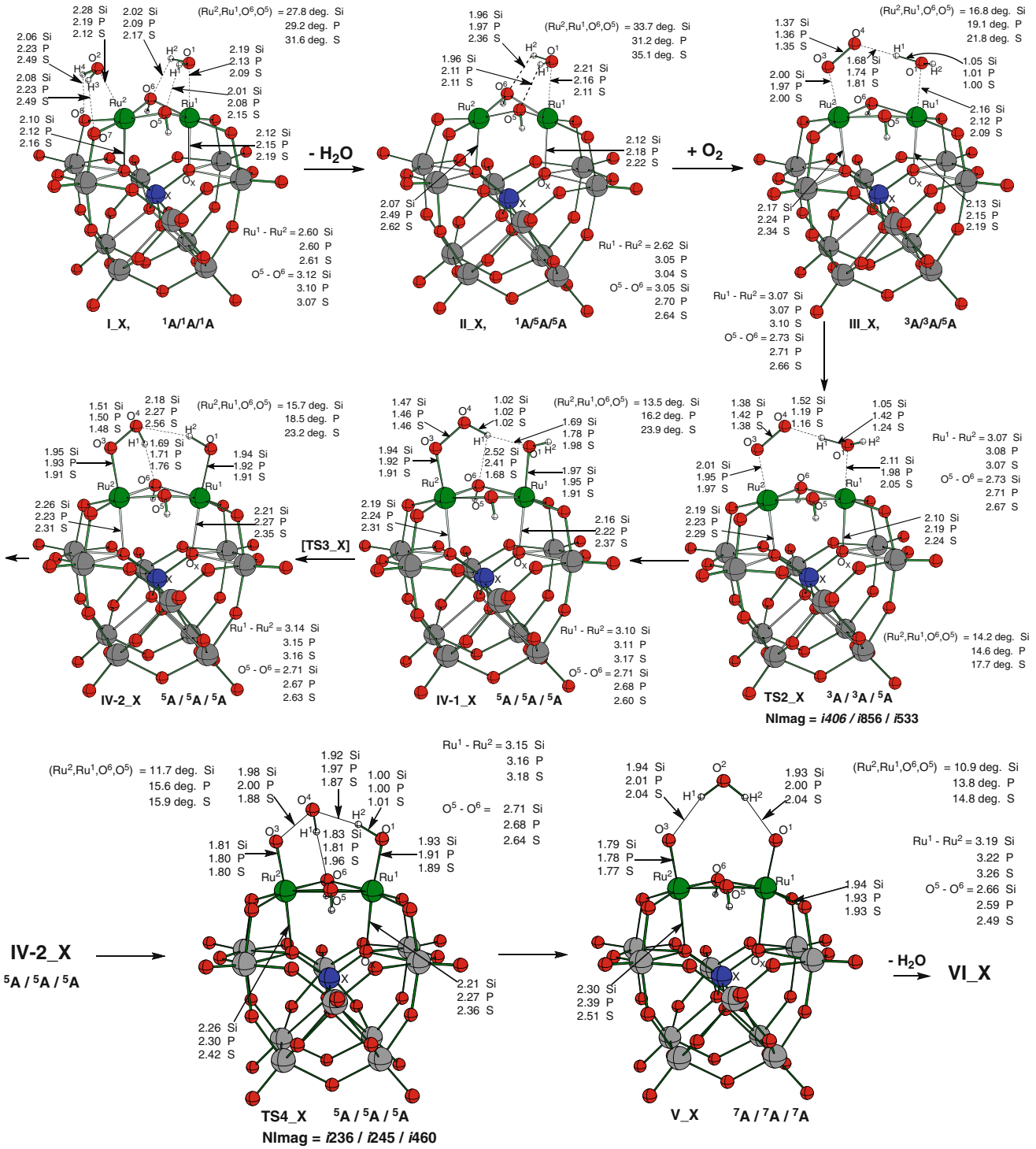

Fig. 1 Calculated important geometry parameters (distances in Å, angles in deg.) of the reactants, transition states, intermediates, and products of the stepwise pathway for the reaction $\{\gamma\text{-}[(H_2O)Ru^{III}(\mu\text{-}OH)_2Ru^{III}(H_2O)][X^{n+}W_{10}O_{36}]\}^{(8-n)-} + O_2 \rightarrow \{\gamma\text{-}[(^{\cdot}O)Ru^{IV}(\mu\text{-}OH)_2 Ru^{IV}(O^{\cdot})][X^{n+}W_{10}O_{36}]\}^{(8-n)-} + 2H_2O$, for X = Si (taken from Ref. [18]), P, and S. Electronic states and imaginary frequencies (for the transition states) are presented as for X = Si/P/S

bond distances are longer by 0.45/0.43, 0.03/0.02, 0.03/0.03, and 0.37/0.46 Å, respectively, but the O^5–O^6 distance is shorter by 0.40/0.43 Å than those in the pre-reaction complex **I_P/I_S,** respectively. Mulliken analysis of **II_P/II_S** shows highly non-symmetrical distribution of spin density over Ru centers (see Table 1). The Ru^1 center bears

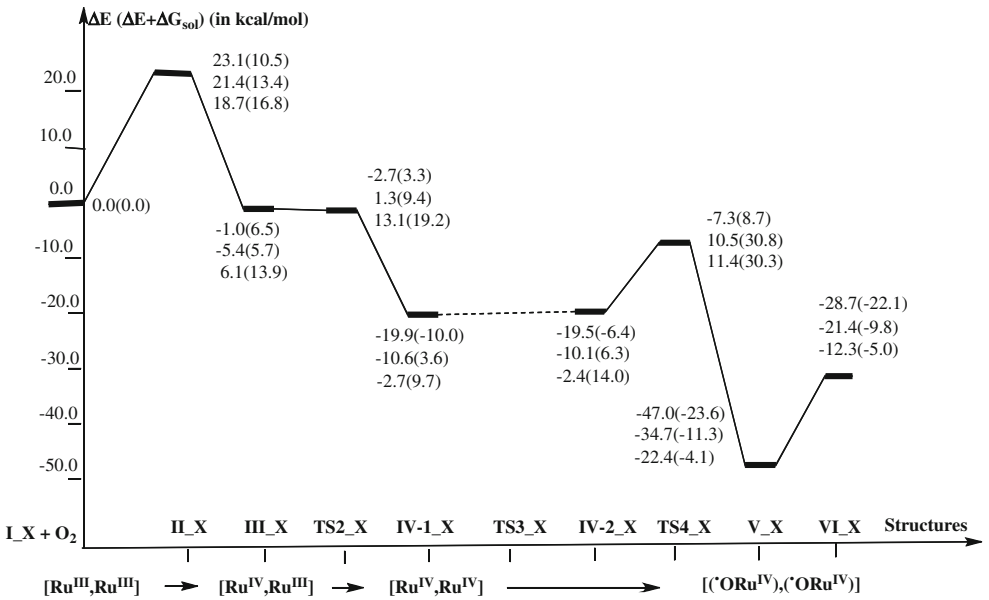

Fig. 2 Schematic presentation of the potential energy surfaces of the reaction $\{\gamma\text{-}[(H_2O)Ru^{III}(\mu\text{-}OH)_2Ru^{III}(H_2O)][X^{n+}W_{10}O_{36}]\}^{(8-n)-} + O_2 \rightarrow \{\gamma\text{-}[(^{\cdot}O)Ru^{IV}(\mu\text{-}OH)_2Ru^{IV}(O^{\cdot})][X^{n+}W_{10}O_{36}]\}^{(8-n)-} + 2H_2O$ for $X = Si$ (taken from Ref. [18]), P and S. The presented relative energies ΔE (and $\Delta E + \Delta G_{solv(water)}$ in *parentheses*) are given in kcal/mol. The numbers for $X = Si$, P, and S are presented in the 1st, 2nd, and 3rd lines, respectively

Table 1 The Mulliken atomic spin densities (in e) of the important atoms, as well as $\langle S^2 \rangle$ values of the ground state intermediates, transition states and products of the reaction (1) for $X = P$ (before slash, "/") and S (after slash, "/")

	II_X	III_X	TS2_X	IV-1_X	IV-2_X	TS4_X	V_X
Ru^1	0.79/0.76	0.84/0.81	1.41/0.90	1.40/1.38	1.40/1.45	1.39/1.38	1.62/1.62
Ru^2	2.48/2.48	1.36/1.38	0.51/1.34	1.22/1.18	1.29/1.25	1.51/1.45	1.62/1.62
O^1	-0.01/−0.01	−0.01/0.01	0.06/0.00	0.12/0.16	0.21/0.17	0.25/0.25	0.87/0.84
O^3	–	−0.38/0.38	−0.48/0.44	0.35/0.35	0.26/0.23	0.70/0.55	0.87/0.84
O^4	–	−0.58/0.57	−0.24/0.38	0.11/0.10	−0.03/0.03	−0.73/−0.57	0.02/0.02
O^5	0.00/0.00	0.05/0.01	0.07/0.03	0.08/0.09	0.07/0.03	0.08/0.09	0.07/0.06
O^6	0.05/0.05	0.08/0.12	0.03/0.15	0.04/−0.01	0.03/0.03	0.05/0.06	0.07/0.06
O^7	0.09/0.32	0.26/0.41	0.10/0.43	0.13/0.13	0.13/0.13	0.17/0.19	0.21/0.22
O^8	0.30/0.08	0.17/0.09	0.08/0.12	0.12/0.18	0.21/0.18	0.25/0.25	0.21/0.22
$\langle S^2 \rangle$	6.02/6.02	2.82/6.02	2.99/6.02	6.02/6.03	6.02/6.02	6.62/6.41	12.04/12.04

0.79/0.76 e of spin density (α-spin), whereas the Ru^2 center bears 2.48/2.48 e (α-spin), and 0.73/0.76 e is distributed over the POM framework atoms, especially on the oxo centers that bridge Ru and W atoms. Thus, formally the Ru^1 center could be considered as low-spin Ru^{III}, while the Ru^2 center could be considered to be an intermediate-spin (quartet, 3 spins) Ru^{III}.

Charges at the Ru centers also increase upon water dissociation compared to the singlet **I_P/I_S** species, slightly from 0.73/0.74 e to 0.77/0.79 e at the Ru^1 center and substantially from 0.56/0.62 e to 0.92/0.97 e at the Ru^2 center. Comparison between the *singlet* **II_P/II_S** (see Table 2) and *singlet* **I_P/I_S** species shows insignificant geometry changes, in very close similarity to the $X = Si$ case; [18] the Ru^1–Ru^2 bond distance is elongated by mere 0.02/0.01 Å and O^5–O^6 distance is shortened by 0.09/0.13 Å, respectively. Ru^1–O^1 and Ru^1–O_X bond distances remain unchanged. The Ru^2–O_X bond distance, after the water molecule dissociation from the Ru^2 center, is shortened by 0.04/0.06 Å.

3.2.2 *Intermediate **III_X**: the O_2 coordination to **II_X***

The next intermediate on the reaction pathway is the product of O_2 coordination to **II_X**, the complex $\{\gamma\text{-}[(O_2)Ru^{III}(\mu\text{-}OH)_2Ru^{III}(H_2O)][X^{n+}W_{10}O_{36}]\}^{(8-n)-}$, **III_X**.

Table 2 The Mulliken atomic charges (in e) of the important atoms of the calculated ground state intermediates, transition states and products of the reaction (1) for $X = P$ (before slash, "/") and S (after slash, "/")

	I_X, ^{1}A/^{1}A	**II_X, ^{3}A/^{5}A**	**III_X, ^{3}A/^{5}A**	**TS2_X, ^{5}A/^{5}A**	**IV-1_X, ^{5}A/^{5}A**	**IV-2_X, ^{5}A/^{5}A**	**TS4_X, ^{5}A/^{5}A**	**V_X, ^{7}A/^{7}A**
Ru^1	0.73/0.74	0.77/0.79	0.80/0.85	0.96/0.87	0.93/1.01	0.99/1.00	0.99/1.02	1.11/1.20
Ru^2	0.56/0.62	0.92/0.97	0.98/1.02	0.91/1.02	0.96/1.01	0.97/0.98	1.01/1.07	1.11/1.20
O^1	−0.64/−0.63	−0.63/−0.62	−0.66/−0.65	−0.66/−0.69	−0.64/−0.54	−0.56/−0.53	−0.56/−0.53	−0.42/−0.35
O^2	−0.65/−0.65	–	–	–	–	–	–	–
O^3	–	–	−0.17/−0.16	−0.18/−0.15	−0.22/−0.19	−0.24/−0.21	−0.28/−0.25	−0.42/−0.35
O^4	–	–	−0.21/−0.19	−0.32/−0.23	−0.36/−0.32	−0.39/−0.35	−0.45/−0.43	−0.79/−0.77
							0.03/0.06[a]	
O^5	−0.63/−0.61	−0.71/−0.70	−0.64/−0.64	−0.66/−0.63	−0.66/−0.73	−0.66/−0.66	−0.66/−0.68	−0.69/−0.76
O^6	−0.63/−0.61	−0.72/−0.70	−0.66/−0.69	−0.64/−0.69	−0.64/−0.74	−0.72/−0.72	−0.71/−0.70	−0.69/−0.76
O^7	−0.65/−0.64	−0.64/−0.66	−0.61/−0.60	−0.60/−0.58	−0.61/−0.61	−0.60/−0.61	−0.60/−0.62	−0.61/−0.62
O^8	−0.65/−0.64	−0.65/−0.65	−0.61/−0.61	−0.60/−0.61	−0.61/−0.62	−0.61/−0.62	−0.60/−0.62	−0.61/−0.62

[a] Total charge (in e) of the transferring O^4H^1-fragment

Complex **III_P** is found to have the triplet ground electronic state, as in the case of **III_Si** [18], whereas the complex **III_S** is found to have the quintet ground electronic state, again in agreement with the fact that S^{VI} favors higher-spin electronic states [33, 34]; the triplet state of **III_S** was calculated to be 2.4 (2.4) kcal/mol higher than its quintet state. The calculated $\langle S^2 \rangle$ values are 6.02 for both complexes. As seen in Figs. 1 and 2, the overall ground state-to-ground state H_2O-to-O_2 substitution reaction, i.e. **I_X** → **II_X** → **III_X**, is found to be *exothermic* by 5.4 kcal/mol in the gas phase for $X = P$, but *endothermic* by 6.1 kcal/mol for $X = S$. In water, it is calculated to be endothermic for both heteroatoms: (5.7) and (13.9) kcal/mol for $X = P$ and S, respectively. Comparison of these results for $X = P$ and S with −1.0 (6.5) kcal/mol reported earlier for $X = Si$ [18] shows that the driving force for the overall H_2O-to-O_2 substitution slightly reduces via $X = P > Si > S$, which can be explained by the geometry change upon going from **I_X** to **III_X** (specially the change in Ru^2–O_X bond distance, see below).

As seen in Fig. 1, the coordination of O_2 to the *ground-state quintet* **II_P** and **II_S** to form the corresponding **III_P** (^{3}A) and **III_S** (^{5}A) species results in significant shortening of the Ru^2–O_X bond distances: from 2.49 to 2.24 Å for $X = P$ and from 2.62 to 2.34 Å for $X = S$. However, the calculated Ru^2–O_S distance in **III_S** (^{5}A) is still quite long, 2.34 Å, implying no bonding between the Ru^2 and O_S centers. It is worth noting that for $X = Si$, in contrast to the $X = P$ and S, the Ru^2–O_{Si} bond distance elongates from 2.07 to 2.17 Å upon the O_2 coordination to **II_Si**, which leads to slight destabilization (rather than stabilization as it is the case for $X = P$) of the resulting **III_Si** intermediate. This trend in change in the calculated Ru^2–O_X distance upon the coordination of O_2 to **II_X** is consistent with the reported exothermicity of the reaction **II_X** + O_2 → **III_X,** which reduces via $X = P$ [26.8 (7.7) kcal/mol] > Si [24.1 (4.0) kcal/mol] [18] > S [12.6 (2.9) kcal/mol].

As shown previously [18] for $X = Si$, the coordination of O_2 to Ru^2 in **II_X** flattens the entire {$Ru(\mu$-$OH)_2Ru$} core; the calculated (Ru^2, Ru^1, O^6, O^5) dihedral angles in **III_X** are 16.8°, 19.1°, and 21.8° versus 33.7°, 31.2°, and 35.1° in **II_X**, for $X = Si$, P, and S, respectively. As seen in Fig. 1, in **III_X**, the oxygen molecule is coordinated to the Ru^2-atom with one of its O-atoms, and its other O-atom is H-bonded to the Ru^1-coordinated water molecule; the Ru^2–$O^3(O_2)$ and O^4–H^1 bond distances are calculated to be 2.00, 1.97, and 2.00 Å, and 1.68, 1.74, and 1.81 Å, respectively, for $X = Si$, P and S. Elongation of the O^4–H^1 bond distance in cases of $X = P$ and S versus $X = Si$ could be explained by slightly smaller Mulliken charge at the O^4 center in **III_P/III_S** (−0.21/−0.16 e) compared to **III_Si** (−0.25 e). The calculated O^3–O^4 bond distance in **III_X** is 1.37, 1.36 and 1.35 Å for $X = Si$, P and S, respectively, by 0.15–17 Å longer than that in the free dioxygen molecule, which implies superoxo character of the coordinated O_2-unit. Indeed, the calculations performed at the same level of theory gave 1.42 and 1.68 Å for O–O bond distances in free $O_2^{-\cdot}$ and O_2^{2-} species, which is in reasonable agreement with experimental value of 1.35 Å for $O_2^{-\cdot}$ [58, 60] and calculated values of 1.64 Å (with the SD-CI approach) and 1.67 Å (with the SAC-CI approach) [59] for O_2^{2-}, respectively. The superoxide character of the O_2-unit in **III_X** is also supported by the results of spin density analysis; the O_2 unit bears about one unpaired spin (0.38 e on the O^3-atom and 0.57–0.58 e on O^4) (Table 1).

The Ru^2 and Ru^1 atoms of **III_P/III_S** bear 1.36/1.38 e and 0.84/0.81 e α-spin density, respectively, and about

0.76/0.84 e α-spin density is delocalized over other atoms. It should be noted that the calculated $\langle S^2 \rangle$ value for the triplet **III_P** is 2.82, which is significantly larger than its ideal value of 2.0. As in the case of **III_Si** [18], this indicates some mixing of high-spin states into the triplet **III_P**; the calculated quintet state of **III_P** has a very similar geometry and lies only 5.1 (5.7) kcal/mol higher in energy than its ground triplet state; in the quintet state, the superoxo unit bears about 1.0 e α-spin density (rather than β-spin density in the triplet). Nevertheless, the calculated exchange coupling constant, J, is only 19.9 cm^{-1}. As seen in Table 1, in the *ground quintet state* **III_S**, the Ru^2 and Ru^1 centers are ferromagnetically coupled both with each other and with the O^3–O^4 superoxo unit. The calculated $\langle S^2 \rangle$ value is 6.02. These results show that in both **III_P** and **III_S**, the Ru^2 and Ru^1 centers could be considered as having oxidation states of +4 (with two spins) and +3 (with one spin), respectively, i.e., upon water substitution by O_2, the Ru^2-center of **II_P/II_S** is oxidized by one electron.

3.2.3 The H-atom transfer: transition state *TS2_X*

From the complex **III_X**, the reaction proceeds via the H-atom (H^1) transfer transition state **TS2_X** to give the hydroperoxo-hydroxo complex $\{\gamma\text{-}[(OOH)Ru^{IV}(\mu\text{-}OH)_2 Ru^{IV}(OH)][X^{n+}W_{10}O_{36}]\}^{(8-n)-}$, **IV_X** (Fig. 1). Calculations show that the transition states **TS2_P/TS2_S** have triplet/quintet ground electronic states as their pre-reaction complexes **III_P/III_S,** respectively. The atoms of the activated superoxo unit O^3–O^4 in **TS2_P/TS2_S** bear spin densities of 0.48/0.44 e on the O^3 and 0.24/0.38 e on the O^4 (see Table 1). However, in **TS2_P**, similar to **III_P**, these spins are antiferromagnetically coupled with spins on the Ru centers, while in **TS2_S**, similar to **III_S**, they are ferromagnetically coupled with spins on the Ru centers. The Mulliken charge (see Table 2) on the transferred H^1 atom in **TS2_P/TS2_S** is +0.46/+0.46 e. Comparison of important geometry parameters of **TS2_P/TS2_S** with those of **III_P/III_S** shows the following: (a) in **TS2_P/TS2_S** the dissociating O^1–H^1 bond becomes significantly elongated, by 0.41/0.24 Å, (b) the forming Ru^1–O^1 and O^4–H^1 bonds are shortened by 0.14/0.04 and 0.55/0.65 Å, respectively, (c) the O^3–O^4 and Ru^2–O^3 bond distances are elongated by 0.06/0.03 Å and shortened by 0.02/0.03 Å, respectively, and (d) Ru^1–O_X and Ru^2–O_X bond distances are elongated by 0.04/0.05 Å and shortened by 0.01/0.05 Å, respectively. Also, the $\{Ru(\mu\text{-}OH)_2Ru\}$ unit in **TS2_P/TS2_S** is further flattened compared with the complex **III_P/III_S**. As can be seen, geometry changes upon going from **III_P/III_S** to the transition state **TS2_P/TS2_S** are quite significant; therefore, **TS2_P/TS2_S** should be considered as a late transition state. In contrast, for X = Si, these changes were found to be relatively insignificant, and the located **TS2_Si** is concluded to be an early transition state [18]. The energy of transition states **TS2_P/TS2_S** relative to **III_P/III_S** are 6.7 (3.7) and 7.0 (5.3) kcal/mol. Thus, these energy barriers are slightly higher for X = P and S than for X = Si, which previously was reported to be −1.7 (−3.2) kcal/mol [18] but still should be considered as small.

3.2.4 The H-atom transfer: hydroperoxo-hydroxo intermediates *IV_X*

Overcoming of the barrier at **TS2_X** leads to the formation of the quintet hydroperoxo-hydroxo intermediates **IV-1_X** (Fig. 1). For X = P, our extensive studies showed the existence of an almost degenerate quintet state and an antiferromagnetically coupled open-shell singlet state; the latter state is by mere 0.1 (0.4) kcal/mol lower than the quintet state. For X = S, we have found a low-lying triplet state located by 2.4 (3.4) kcal/mol higher than the quintet ground state. Its closed-shell singlet was found to be 10.8 (12.0) kcal/mol higher than the quintet ground state.

The calculated Ru^1–O^1 (1.95/1.91 Å) and Ru^2–O^3 (1.92/1.91 Å) bond distances in **IV-1_P/IV-1_S** show the existence of the covalent bonding between the Ru centers and OOH and OH groups, respectively, similar to the case of **IV-1_Si** structure [18]. During the reaction **III_X** → **TS2_X** → **IV-1_X**, (a) the geometry of the $\{Ru(\mu\text{-}OH)_2Ru\}$ core and the Ru^2–O_X bond distance change only slightly, (b) the Ru^1–O_X bond distance elongates by 0.03, 0.07 and 0.18 Å, and (c) the formed Ru^1–O^1 and Ru^2–O^3 bond distances shorten by 0.06, 0.05, 0.09 Å, and 0.19, 0.17, 0.18 Å, for X = Si, P and S, respectively. Interestingly, in contrast to X = Si and P, in **IV-1_S** H^1 can form only very weak, if any, hydrogen bond to the terminal O^1H^2-ligand; the calculated H^1–O^2 distance is 1.69, 1.78, and 2.98 Å, for X = Si, P, and S, respectively. Comparison of the presented geometry changes along the reaction **III_X** → **TS2_X** → **IV-1_X**, for X = Si, P and S shows that the X = S species acquires pronounced "out-of-pocket" configuration.

The Mulliken charges and spin densities are significantly changed during the reaction **III_X** → **TS2_X** → **IV-1_X**: (1) the total spin density on the O^3–O^4 moiety changes from −0.96 e (β-spin) to 0.46 e (α-spin) for X = P and from 0.95 e (α-spin) to 0.45 e (α-spin) for X = S; (2) the total spin density on the Ru^1 and Ru^2 atoms increases from 2.2 e to 2.62 e (α-spins), for X = P, and from 2.19 e to 2.56 e (α-spins), for X = S, (3) about 0.87, 0.92, and 0.99 e spin is distributed over the framework atoms for X = Si [18], P and S, respectively. Both Ru^1 and Ru^2 of **IV-1_X** can be considered formally as Ru^{IV} for all three

X's. We were also able to locate the antiferromagnetically coupled open-shell singlet state of **III-1_P**, which has geometry very similar to the quintet state, with spin densities 1.41 e (α-spin) at the Ru^1 center and 1.22 e (β-spin) at the Ru^2 center and 0.45 e (β-spin) on the O^3–O^4 moiety. Cartesian coordinates and full results of Mulliken analysis of the antiferromagnetically coupled open-shell singlet are provided in Supporting Information (see Table S4 and S5, respectively). Formation of the hydroperoxo-hydroxo species **IV-1_P/IV-1_S** is found to be exothermic by 5.2 (2.1)/8.8 (4.2) kcal/mol, calculated relative to the complex **III_P/III_S**, respectively (see Fig. 2). These values are smaller than the 18.9 (16.5) kcal/mol reported for $X = Si$ [18].

Further, the intermediates **IV-1_X** rearrange into isomers **IV-2_X**, where bridging O^6H-group is H-bonded to the OOH-group [18]. Calculations show that both **IV-2_P/IV-2_S** have the quintet ground state as previously studied **IV-2_Si** [18] and are located only 0.5 (2.7)/0.3 (4.3) kcal/mol higher in energy than the **IV-1_P/IV-1_S** isomers, respectively. During the **IV-1_X** → **IV-2_X** rearrangement, the O^1H^2-group is rotated around the Ru^1–O^1, which is expected to proceed via a small rotational barrier [18]. As in the case for $X = Si$ [18], we were not able to locate the transition state (**TS3_X**) associated with this barrier. Comparison of the calculated geometries of **IV-1_P/IV-1_S** and **IV-2_P/IV-2_S** shows that in the latter, the Ru^1–Ru^2, O^3–O^4, Ru^1–O^6, and Ru^2–O^6 bond distances are elongated by 0.04/0.01, 0.04/0.02, 0.03/0.03, and 0.05/0.03 Å, respectively. The calculated H^1–O^6, Ru^1–O^1, and Ru^2–O^3 bond distances are shortened by 0.70, 0.03, and 0.01 Å, for $X = P$. For the $X = S$, the H^1–O^6 bond distance elongates by 0.08 Å, and the Ru^1–O^1 and Ru^2–O^3 bond distances do not change at all. In **IV-2_S**, the H^2–O^4 distance is calculated to be 2.56 Å, i.e., by 0.38 and 0.29 Å longer than in **IV-2_P** and **IV-2_Si**, respectively, which again could be explained by more pronounced "out-of-pocket" configuration of **IV-2_S**.

3.2.5 *The water formation: transition state* ***TS4_X***

From the intermediate **IV-2_X**, the reaction proceeds to the formation of water, $O^4H^1H^2$ and the product complex $\{\gamma$-$[(O)Ru(\mu\text{-}OH)_2Ru(O)](H_2O)[X^{n+}W_{10}O_{36}]\}^{(8-n)-}$, **V_X**, containing an $\{ORu(\mu\text{-}OH)_2RuO)\}$ core (the next 2 e-oxidation step) (Fig. 1). This reaction proceeds via the transition state **TS4_X**, which is found to have a quintet ground state for all three *X* atoms, as the pre-reaction complexes **IV-1_X** and **IV-2_X**. As mentioned above, isomers **IV-1_X** and **IV-2_X** are energetically close to each other and separated with a small energy barrier. Therefore, we calculate barriers at the **TS4_X** from the energetically most stable intermediate **IV-1_X**. These energy barriers are 12.6 (18.7), 21.1 (27.2), and 14.1 (20.6) kcal/mol for $X = Si$ [18], P, and S, respectively (see Fig. 2). The comparison of the calculated bond distances of O^3–O^4 = 2.00/1.88 Å, O^4–H^2 = 1.97/1.87 Å, H^1–O^6 = 1.81/1.96 Å, and Ru^2–O^3 = 1.80/1.80 Å, for **TS4_P/TS4_S**, with their values in the pre-reaction complex **IV-2_P**, shows that in **TS4_P/TS4_S** the O^3–O^4, O^1–H^2, and H^1–O^6 bonds are dissociated, and the Ru^2–O^3 and H^2–O^4 bonds are formed in a concerted fashion. Based on these geometry analyses, one may describe the **TS4_P/TS4_S** transition state as an OH-transfer transition state rather than a proton transfer one, as in the case of the transition state **TS4_Si** [18]. In **TS4_X**, the total charge of the moving OH-group is calculated to be very small (Table 2). Spin density analysis shows that in the ground quintet state of **TS4_X**, the O^3–O^4 bond acquires significant biradical character (Table 1); the oxygen atoms, originated from the dioxygen molecule, bear significant fractions of unpaired spin density with opposite signs, implying the O–O bond breaking at the transition state. The $\{Ru(\mu\text{-}OH)_2Ru\}$ core is noticeably flattened in **TS4_X**, in comparison with **IV-2_X**, although the Ru^1–Ru^2, Ru^1–O^5, Ru^2–O^6 bond distances are changed only slightly (Fig. 1).

The calculated geometries of **TS4_X** are closer to those of the reactants **IV-2_X**; therefore, **TS4_X** should be considered as early transition states, as expected for an highly exothermic reaction; the **IV-2_X** → **TS4_X** → **V_X** transformation is calculated to be exothermic by 27.1 (13.6) [18], 24.1 (14.9), and 19.7 (13.8) kcal/mol for $X = Si$, P, and S, respectively (Fig. 2).

3.2.6 *The final products* ***V_X*** *and* ***VI_X***

The resulting complexes **V_X** have a septet ground electronic state for all studied *X*, and the formed H_2O^4 molecule formed is H-bonded to their Ru = O units. Similar to the previously studied **V_Si** complex [18], the spin density analysis (see Table 1) shows that the **V_P** and **V_S** also have a strong biradicaloid character. In these complexes, the Ru centers bear spin density of 1.62 e each, and their O^1 and O^3 centers (oxo oxygens) have 0.87 e ($X = P$)/0.84 e ($X = S$) spins each. All unpaired spins in **V_X** are α-spins. Thus, again, as in previously studied $X = Si$ case [18], the final complexes **V_X** for $X = P$ and S should be formulated as species with the Ru^{IV}-$O^{\cdot}$ units, rather than species having the $Ru^V = O$ groups. In **V_P/V_S**, the Ru^1–Ru^2 bond distance is elongated by 0.07/0.10 Å, while O^5–O^6 bond distance is shortened by 0.08/0.14 Å in comparison with the reactant **IV-2_P/IV-2_S**. The most drastic changes, however, occur in Ru^1–O^1 and Ru^2–O^3 bond distances; they are shortened by 0.14/0.14 and 0.15/0.14 Å, upon going from **IV-2_P/IV-2_S** to **V_P/V_S**. This indicates the formation of RuO unit with multiple

ruthenium-oxygen bond character in **V_X**. In **V_P/V_S** elongates the Ru–O_X bond distances up to 2.39/2.51 Å, thus dictating a pronounced "out-of-pocket" configuration to the complex **V_X**. Interestingly, the H^1–O^3 and H^2–O^1 bond distances in **V_X** species are steadily elongated from $X = Si$ (1.94 and 1.93 Å, respectively) to P (2.01 and 2.00 Å, respectively) to S (2.04 Å).

Dissociation of H-bonded water molecule from **V_X** leads to final product **VI_X**. Since geometry and electronic structure of **VI_X** are very close to those of **V_X**, we will not discuss them here: they are presented in Supporting Materials.

4 Discussion

The overall potential energy surface of the reaction (1), i.e., the reaction of di-Ru-substituted γ-Keggin polyoxotungstate $\{\gamma\text{-}[(H_2O)Ru^{III}(\mu\text{-}OH)_2Ru^{III}(H_2O)][(X^{n+}W_{10}O_{36}]\}^{(8-n)-}$, **I_X** (where $X = Si$, P and S), with O_2 molecule, is presented in Fig. 2. As seen from Fig. 2, this reaction is exothermic by 28.7 (22.1), 21.4 (9.8), and 12.3 (5.0) kcal/mol for $X = Si$, P, and S, respectively. In other words, the exothermicity of the reaction (1) reduces upon changing heteroatom via $X = Si > P > S$.

As mentioned above, this reaction is a 4-electron oxidation process. Its first step is the H_2O-to-O_2 substitution that transforms the reactant $\{\gamma\text{-}[(H_2O)Ru^{III}(\mu\text{-}OH)_2Ru^{III}(H_2O)][(X^{n+}W_{10}O_{36}]\}^{(8-n)-}$, **I_X**, to the $\{\gamma\text{-}[(OO)Ru^{IV}(\mu\text{-}OH)_2Ru^{III}(H_2O)][(X^{n+}W_{10}O_{36}]\}^{(8-n)-}$, **III_X** intermediate with the superoxide ($OO^{-\cdot}$) ligand (the first 1 e-oxidation step). This step may proceed via the stepwise/dissociative and concerted/associative pathways, which lead to the same conclusions. The stepwise pathway occurs via the dissociation of the water molecule from **I_X** to form $\{\gamma\text{-}Ru^{III}(\mu\text{-}OH)_2Ru^{III}(H_2O)][X^{n+}W_{10}O_{36}]\}^{(8-n)-}$, **II_X**, followed by the addition of O_2 to the coordinatively unsaturated Ru center to form the intermediate **III_X**. In the concerted pathway, the H_2O-to-O_2 substitution occurs in a single step via a concerted transition state **TS1_X**. Despite substantial efforts, we were not able to locate the H_2O-to-O_2 substitution transition state **TS1_X**. In any case, the upper limit of the H_2O-to-O_2 substitution barrier is the energy required for the water dissociation from **I_X**, which is calculated to be 23.1 (10.5), 21.4 (13.4), and 18.7 (16.8) kcal/mol for $X = Si$, P, and S, respectively. The energy of the H_2O-to-O_2 substitution reaction, **I_X** + O_2 → **III_X** + H_2O, is found to reduce in the following sequence: $X = P$ [−5.4 (5.7) kcal/mol] > Si [−1.0 (6.5) kcal/mol] > S [6.1 (13.9) kcal/mol]. This trend can be explained by stabilization of the Ru^2–O_X bond distance upon going from **II_X** to **III_X** for $X = P$ and S, but its destabilization for $X = Si$.

The next step of the reaction is the proton transfer from the coordinated H_2O molecule to the superoxide ($OO^{-\cdot}$) unit in **III_X** to form the hydroperoxo-hydroxo intermediate $\{\gamma\text{-}[(OOH)Ru^{IV}(\mu\text{-}OH)_2Ru^{IV}(OH)][X^{n+}W_{10}O_{36}]\}^{(8-n)-}$, **IV-1_X** (the second 1 e-oxidation), followed by **IV-1_X** → **IV-2_X** isomerization and occurs with a maximum of −1.7 (−3.2), 6.7 (3.7) and 7.0 (5.3) kcal/mol energy barrier at the transition state **TS2_X**, for $X = Si$, P and S, and is a facile process.

From the intermediate **IV-2_X** (or its energetically more stable isomer **IV-1_X)**, the reaction proceeds via the O–OH bond cleavage followed by the spontaneous formation of the water molecule and two Ru = O bonds. The resulting product, $(H_2O)\cdots\{\gamma\text{-}[(^{\cdot}O)Ru^{IV}(\mu\text{-}OH)_2Ru^{IV}(O^{\cdot})][X^{n+}W_{10}O_{36}]\}^{(8-n)-}$, **V_X**, is formulated to be a radical species with two $Ru^{IV} = O^{\cdot}$ units. Similar biradicaloidal character of the Ru = O-fragments of the $\{(bpy)_2[(^{\cdot}O)Ru^{IV}(\mu\text{-}O)Ru^{IV}(O^{\cdot})](bpy)_2\}^{4+}$ intermediate of the "blue-dimer" was reported by Yang and Baik [19]. As seen in Fig. 2, this step of the reaction, i.e., the **IV-1_X** → **TS4_X** → **V_X** transformation, is exothermic by 27.1 (13.6) [18], 24.1 (14.9), and 19.7 (13.8) kcal/mol and occurs with a 12.6 (18.7), 21.1 (27.2), and 14.1 (20.6) kcal/mol energy barrier at the transition state **TS4_X,** for $X = Si$ [18], P, and S, respectively. Comparison of these barriers with those reported for the H_2O-to-O_2 substitution step [23.1 (10.5), 21.4 (13.4), and 18.7 (16.8) kcal/mol for $X = Si$, P, and S, respectively] shows that the former are smaller (almost the same for $X = P$) in the gas phase but are somewhat larger in water. In other words, in the gas phase, the rate-determining step of overall reaction (1) is the H_2O-to-O_2 substitution step, while in the water solution, the pre-final step, i.e., the O–OH bond cleavage and formation of the two Ru = O bonds, becomes the kinetically most demanding step for the reaction (1). As a result, the hydroperoxo-hydroxo intermediate **IV-1_X** of the reaction (1) becomes a kinetically stable species for all studied X, especially for $X = P$.

At the final step, the dissociation of the formed water molecule from **V_X** occurs, i.e. **V_X** → $\{\gamma\text{-}[(^{\cdot}O)Ru^{IV}(\mu\text{-}OH)_2Ru^{IV}(O^{\cdot})][(X^{n+}O_4)W_{10}O_{32}]\}^{(8-n)-}$ (**VI_X**) + H_2O, which requires 18.3 (1.5), 13.3 (−1.5), and 10.1 (−0.9) kcal/mol for $X = Si$, P, and S, respectively (negative values indicate that this reaction is exothermic).

Thus, the above presented discussion shows that reaction (1) is a kinetically and thermodynamically facile process for all studied X. The "reverse" reaction, i.e., O_2 formation by reaction of water with $\{\gamma\text{-}[(^{\cdot}O)Ru^{IV}(\mu\text{-}OH)_2Ru^{IV}(O^{\cdot})][(X^{n+}W_{10}O_{36}]\}^{(8-n)-}$ is an endothermic process by 28.7 (22.1), 21.4 (9.8), and 12.3 (5.0) kcal/mol for $X = Si$, P, and S, respectively. In other words, the water oxidation by the complex $\{\gamma\text{-}[(^{\cdot}O)Ru^{IV}(\mu\text{-}OH)_2Ru^{IV}(O^{\cdot})][(X^{n+}W_{10}O_{36}]\}^{(8-n)-}$ is unlikely for $X = Si$ and P, while it

could occur for $X = S$ at specific conditions. This conclusion is drastically different from that reported for the "blue-dimer" $\{(bpy)_2[^{\cdot}ORu^{IV}(\mu\text{-}O)Ru^{IV}(O^{\cdot})](bpy)_2\}^{4+}$ intermediate, which oxidizes the incoming water molecule to produce O_2 [19–32]. This difference in reactivity of $\{\gamma\text{-}[(^{\cdot}O)Ru^{IV}(\mu\text{-}OH)_2Ru^{IV}(O^{\cdot})][(SiW_{10}O_{36}]\}^{4-}$ and its "blue-dimer" analog $\{(bpy)_2[^{\cdot}ORu^{IV}(\mu\text{-}O)Ru^{IV}(O^{\cdot})](bpy)_2\}^{4+}$ toward H_2O molecule has been explained in terms of the electron-rich nature (better σ donor and π acceptor character) of $[SiW_{10}O_{36}]^{4-}$ relative to *bpy* [18].

It is noteworthy that the lack of reactivity of the $\{\gamma\text{-}[(^{\cdot}O)Ru^{IV}(\mu\text{-}OH)_2Ru^{IV}(O^{\cdot})][(X^{n+}W_{10}O_{36}]\}^{(8-n)-}$ radical toward the water molecule facilitates its reaction with another $\{\gamma\text{-}[(H_2O)Ru^{III}(\mu\text{-}OH)_2Ru^{III}(H_2O)][(X^{n+}W_{10}O_{36}]\}^{(8-n)-}$ reactant/molecule leading to the formation of $[\{Ru_4^{IV}O_4(OH)_2(H_2O)_4\}[(\gamma\text{-}XW_{10}O_{36}]_2\}^{m-}$ dimer. Our experimental studies (and preliminary calculations) are fully consistent with this prediction. In fact, the dimer $[\{Ru_4^{IV}O_4(OH)_2(H_2O)_4\}[(\gamma\text{-}XW_{10}O_{36}]_2\}^{m-}$ is prepared and carefully studied for the $X = Si$ ($m = 10$) [62, 63] and P ($m = 8$) [64]. It was shown that these dimers are very stable in aqueous solution and catalyze the oxidation of water. More detailed computational studies on the mechanism of the dimerization reaction:

$$\begin{aligned} &VI + \{\gamma - [(H_2O)Ru^{III}(\mu - OH)_2Ru^{III}(H_2O)] \\ &[(X^{n+}OW_{10}O_{36}]\}^{(8-n)-} \\ &\rightarrow [\{Ru_4^{IV}O_4(OH)_2(H_2O)_4\}[(\gamma - XW_{10}O_{36}]_2\}^{m-} + 2H^+, \end{aligned}$$

are in progress.

5 Conclusions

From the above presented data, we can draw the following general conclusions.

1. The nature of the heteroatom X only slightly affects the reactivity of the di-Ru-substituted polyoxotungstates $\{\gamma\text{-}[(H_2O)Ru^{III}(\mu\text{-}OH)_2Ru^{III}(H_2O)][(X^{n+}W_{10}O_{36}]\}^{(8-n)-}$, **I_X** (where $X = Si$, P and S), toward the O_2 molecule. This reaction proceeds with a moderate energy barrier for all studied X's and produces the $\{\gamma\text{-}[(^{\cdot}O)Ru^{IV}(\mu\text{-}OH)_2Ru^{IV}(O^{\cdot})][(X^{n+}W_{10}O_{36}]\}^{(8-n)-}$ radical. The exothermicity of the reaction decreases as $X = Si$ [28.7 (22.1) kcal/mol] > P [21.4 (9.8) kcal/mol] > S [12.3 (5.0) kcal/mol].
2. The "reverse" reaction, namely water oxidation by $\{\gamma\text{-}[(^{\cdot}O)Ru^{IV}(\mu\text{-}OH)_2Ru^{IV}(O^{\cdot})]\ [(X^{n+}W_{10}O_{36}]\}^{(8-n)-}$, is an endothermic process and unlikely to occur for $X = Si$ and P, while it could take place for the $X = S$ under specific conditions.
3. The lack of reactivity of the $\{\gamma\text{-}[(^{\cdot}O)Ru^{IV}(\mu\text{-}OH)_2Ru^{IV}(O^{\cdot})][(X^{n+}O_4)W_{10}O_{32}]\}^{(8-n)-}$ biradical species toward water leads to the formation of stable $[\{Ru_4^{IV}O_4(OH)_2(H_2O)_4\}[(\gamma\text{-}XW_{10}O_{36}]_2\}^{m-}$ dimer. This conclusion is consistent with our experimental findings; the $[\{Ru_4^{IV}O_4(OH)_2(H_2O)_4\}[(\gamma\text{-}XW_{10}O_{36}]_2\}^{m-}$ dimers for the $X = Si$ ($m = 10$) [62, 63] and P ($m = 8$) [64] are stable in aqueous solution and catalyze water oxidation by strong oxidants.

Acknowledgments The present research is supported in part by grant DE-FG02-03ER15461 of U.S. Department of Energy. We also acknowledge NSF grant CHE-0553581 and the Cherry Emerson Center for Scientific Computation.

References

1. Hill CL Guest Ed (1998) Chem Rev 98:1
2. Pope MT, Müller A (eds) (2001) Polyoxometalate chemistry: from topology via self-assembly to applications. Kluwer, Dordrecht
3. Yamase T, Pope MT (eds) (2002) Polyoxometalate chemistry for nano-composite design. Kluwer, Dordrecht
4. Hill CL (2004) In: Wedd AG (ed) Comprehensive coordination chemistry-II: from biology to nanotechnology, vol 4. Elsevier Ltd, Oxford, pp 679–759
5. Pope MT, Müller A (1991) Angew Chem Int Ed 30:34–48
6. Borrás-Almenar JJ, Coronado E, Müller A, Pope MT (2003) Polyoxometalate molecular science, vol 98. Kluwer, Dordrecht
7. Pope MT (2004) In: Wedd AG (ed) Comprehensive coordination chemistry-II: from biology to nanotechnology, vol 4. Elsevier Ltd, Oxford, pp 635–678
8. Hill CL, Prosser-McCartha CM (1995) Coord Chem Rev 143:407–455
9. Okuhara T, Mizuno N, Misono M (1996) Adv Cat 41:113–252
10. Neumann R (1998) Prog Inorg Chem 47:317–370
11. Neumann R (2004) In: Bäckvall JE (ed) Modern oxidation methods, Wiley-VCH, Weinheim, pp 223–251
12. Mizuno N, Yamaguchi K, Kamata K (2005) Coord Chem Rev 249:1944–1956
13. Keita B, Mbomekalle IM, Lu YW, Nadjo L, Berthet P, Anderson TM, Hill CL (2004) Eur J Inorg Chem 17:3462–3475
14. Keita B, Mbomekalle IM, Nadjo L, Anderson TM, Hill CL (2004) Inorg Chem 43:3257–3263
15. Anderson TM, Cao R, Neiwert WA, Hardcastle KI, Hill CL, Ammam M, Keita B, Nadjo L (2005) Eur J Inorg Chem 9:1770–1775
16. Keita B, Mialane P, Sécheresse F, de Oliveira P, Nadjo L (2007) Electrochem Commun 9:164–172
17. Sadakane M, Tsukuma D, Dickman MH, Bassil BS, Kortz U, Capron M, Ueda W (2007) Dalton Trans 26:2833–2838
18. Kuznetsov AE, Geletii YV, Hill CL, Morokuma K, Musaev DGJ (2009) Am Chem Soc 131:6844–6854
19. Yang X, Baik M-HJ (2006) Am Chem Soc 128:7476–7485
20. Gersten SW, Samuels GJ, Meyer TJJ (1982) Am Chem Soc 104:4029–4030
21. Rüttinger W, Dismukes GC (1997) Chem Rev 97:1–24
22. Liu F, Concepcion JJ, Jurss JW, Cardolaccia T, Templeton JL, Meyer TJ (2008) Inorg Chem 47:1727–1752

23. Alstrum-Acevedo JH, Brennmann MK, Meyer TJ (2005) Inorg Chem 44:6802–6827
24. Huynh MHV, Meyer TJ (2007) Chem Rev 107:5004–5064
25. Huynh MHV, Dattelbaum DM, Meyer TJ (2005) Coord Chem Rev 249:457–483
26. Hurst JK, Cape JL, Clark AE, Das S, Qin C (2008) Inorg Chem 47:1753–1764
27. Hurst JK (2005) Coord Chem Rev 249:313–328
28. Romero I, Rodriguez M, Sens C, Mola J, Kollipara MR, Francàs L, Mas-Marza E, Escriche L, Llobet A (2008) Inorg Chem 47:1824–1834
29. Süss-Fink G (2008) Angew Chem Int Ed 47:5888–5890
30. Bartolotti LJ, Pedersen LG, Meyer TJ (2001) Int J Quantum Chem 83:143–149
31. Yang X, Baik M-HJ (2004) Am Chem Soc 126:13222–13223
32. Batista ER, Martin RLJ (2007) Am Chem Soc 129:7224–7225
33. Quiñonero D, Wang Y, Morokuma K, Khavrutskii LA, Botar B, Geletii YV, Hill CL, Musaev DGJ (2006) Phys Chem B 110:170–173
34. Wang Y, Zheng G, Morokuma K, Geletii YV, Hill CL, Musaev DGJ (2006) Phys Chem B 110:5230–5237
35. Quinonero D, Kaledin A, Kuznetsov AE, Geletii YV, Besson C, Hill CL, Musaev DGJ (2010) Phys Chem A 114:535–542
36. Frisch MJ et al (2004) Gaussian 03, revision C1. Gaussian, Inc, Wallingford
37. Becke AD (1988) Phys Rev A 38:3098–3107
38. Lee C, Yang W, Parr RG (1988) Phys Rev B 37:785–789
39. Becke ADJ (1993) Chem Phys 98:1372–1380
40. Hay PJ, Wadt WRJ (1985) Chem Phys 82:270–283
41. Hay PJ, Wadt WRJ (1985) Chem Phys 82:299–310
42. Wadt WR, Hay PJJ (1985) Chem Phys 82:284–298
43. Andrae D, Häußermann U, Dolg M, Stoll H, Preuss H (1990) Theor Chim Acta 77:123–141
44. Yamaguchi K, Takahara Y, Fueno T (1986) Proceedings of Nobel Laureates symposium on Applied Quantum Chemistry. Reidel, Doldrecht, pp 155–184
46. Noodleman L (1981) J Chem Phys 74:5737–5743
47. Noodleman L, Case D (1992) Adv Inorg Chem 38:423–470
48. Musaev DG, Morokuma K, Geletii YV, Hill CL (2004) Inorg Chem 43:7702–7708
49. Ananikov VP, Musaev DG, Morokuma KJ (2010) Mol Cat A 324:104–119
50. Cances E, Mennucci B, Tomasi J (1997) J Chem Phys 107:3032–3041
51. Quiñonero D, Morokuma K, Geletii YV, Hill CL, Musaev DG (2007) J Mol Catal A Chem 262:227–235
52. Pichon C, Mialane P, Dolbecq A, Marrot J, Rivière E, Keita B, Nadjo L, Sécheresse F (2007) Inorg Chem 46:5292–5301
53. Drewes D, Piepenbrink M, Krebs BJ (2006) Cluster Sci 17:361–374
54. Romo S, Fernandez JA, Maestre JM, Keita B, Nadjo L, de Graaf C, Poblet JM (2007) Inorg Chem 46:4022–4027
55. Drewes D, Limanski EM, Krebs B (2004) Dalton Trans 2087–2091
56. Zueva EM, Chermette H, Borshch SA (2004) Inorg Chem 43:2834–2844
57. Botar B, Geletii YV, Kögerler P, Musaev DG, Morokuma K, Weinstock IA, Hill CLJ (2006) Am Chem Soc 128:11268–11277
58. Linstrom PJ, Mallard WG, NIST Chemistry WebBook, NIST Standard Reference Database Number 69, March 2003, National Institute of Standards and Technology, Gaithersburg MD, 20899. Available from: http://webbook.nist.gov
59. Nakatsuji H, Nakai H (1992) Chem Phys Lett 197:339–345
60. Lide DR (ed) (2005) CRC handbook of chemistry and physics, 86th ed. CRC Press, Boca Raton
61. Gilbert JA, Eggleston DS, Murphy WR Jr, Geselowitz DA, Gersten SW, Hodgson DJ, Meyer TJ (1985) J Am Chem Soc 107:3855–3864
62. Geletii YV, Botar B, Kögerler P, Hillesheim DA, Musaev DG, Hill CL (2008) Angew Chem Int Ed 47:3896–3899
63. Geletii YV, Besson C, Hou Y, Yin Q, Musaev DG, Quinonero D, Cao R, Hardcastle KI, Proust A, Kogerler P, Hill CLJ (2009) Am Chem Soc 131:17360–17370
64. Besson C, Huang Z, Geletii YV, Lense S, Hardcastle KI, Musaev DG, Lian T, Proust A, Hill CL (2010) Chem Commun 46:2784–2786